Cambridge Centre for Computational Chemical Engineering

University of Cambridge

Department of Chemical Engineering

Preprint ISSN 1473 – 4273

Towards a Comprehensive Model of the Synthesis of TiO_2 particles from $TiCl_4$.

Richard H. West, Matthew S. Celnik, Oliver R. Inderwildi, Markus Kraft [1] ,

Gregory J. O. Beran, Willam H. Green [2]

released: 26 July 2007

[1] Department of Chemical Engineering
University of Cambridge
Pembroke Street
Cambridge CB2 3RA
UK
E-mail: mk306@cam.ac.uk

[2] Department of Chemical Engineering
Massachusetts Institute of Technology
77 Massachusetts Avenue, 66-270A
Cambridge, MA 02139
USA
E-mail: whgreen@mit.edu

Preprint No. 49

c4e

Key words and phrases: Titania, titanium tetrachloride, kinetic model, mechanism, population balance, primary particle

Edited by
Cambridge Centre for Computational Chemical Engineering
Department of Chemical Engineering
University of Cambridge
Cambridge CB2 3RA
United Kingdom.

Fax: + 44 (0)1223 334796
E-Mail: c4e@cheng.cam.ac.uk
World Wide Web: http://www.cheng.cam.ac.uk/c4e/

Abstract

The combustion of $TiCl_4$ to synthesize TiO_2 nanoparticles is a multi-million tonne per year industrial process. This paper aims to further the understanding of this process. Work towards three aspects of this multi-scale problem is presented herein: gas-phase chemistry, surface chemistry, and the solution of a multidimensional population balance problem coupled to detailed chemical mechanisms.

Presented here is the first thermodynamically consistent mechanism with physically realistic elementary-step rate constants by which $TiCl_4$ is oxidised to form a stable $Ti_2O_xCl_y$ species that lies on the path to formation of TiO_2 nanoparticles. Secondly, progress towards a surface chemistry mechanism based on density functional theory (DFT) calculations is described. Thirdly, the extension of a stochastic 2-dimensional (surface-volume) population balance solver is presented. For the first time the number and size of primary particles within each agglomerate particle in the population is tracked. The particle model incorporating inception, coagulation, growth, and sintering, is coupled to the new gas phase kinetic model using operator splitting, and is used to simulate a heated furnace laboratory reactor and an industrial reactor. Using the primary particle information, TEM-style images of the particles are generated, demonstrating the potential utility of first-principles modelling for the prediction of particle morphology in complex industrial systems.

Contents

1 Introduction

Titanium dioxide (TiO_2) is widely used as a pigment, as a catalyst support, and as a photocatalyst. The combustion of titanium tetrachloride ($TiCl_4$) to synthesize TiO_2 nanoparticles is a multi-million tonne per year industrial process [12]. In this "chloride" process, purified titanium tetrachloride is oxidised at high temperatures (1500–2000 K) in a pure oxygen plasma or flame to produce TiO_2 particles [9, 14].

The size and shape of these particles affects properties important to both the industrial processing and the final product, such as ease of milling[14] and opacity of the powder [9]. Furthermore, the ability to control characteristics of specialised functional nanoparticles through flame synthesis would offer considerable financial reward. As such, the ability to simulate a multi-variate distribution (for example mass, surface area, amount of agglomeration) of a population of nanoparticles created in this process would help efforts to improve the final product and save energy.

Although it has been used in industry for decades,[48] the process is poorly understood and experimental optimization is incremental and costly. It has been demonstrated that the relative rates of gas phase reactions leading to particle nucleation, surface growth reactions, and particle agglomeration and sintering are all important in determining the final product properties [37]. It is important that a comprehensive model includes details spanning all relevant length and time scales.

Existing models greatly simplify the chemical processes to a single step and are unable to capture the details of temperature and concentration dependencies. For example, the use of additives such as $AlCl_3$ and KCl to control the crystal structure and primary particle size of the product is common in industry[1], but current modelling methods can offer no insight into the underlying processes.

As well as detailed chemistry on the molecular scale, it is clear that a detailed population balance model of the particles is desirable. Existing models range from simple monodisperse assumptions to two-dimensional (surface–volume) approaches simulating simultaneous nucleation, growth, agglomeration and sintering. The ability to track primary and agglomerate sizes explicitly will allow the assumptions, such as monodisperse size distributions, currently used to model hard- and soft-agglomerate formation[17] to be relaxed.

This work aims to create and demonstrate a framework for a comprehensive model that attempts to describe the phenomena at different scales. We present new results in three areas:

- Ab-initio and density functional theory (DFT) investigations of the gas phase chemistry of the combustion of $TiCl_4$ lay the foundation for the first detailed kinetic model of seed formation.
- A DFT study of the surface chemistry of rutile TiO_2 is undertaken as a first attempt to understand the surface growth of TiO_2 nanoparticles.
- A new population balance model extends existing surface-volume models, to track primary particles within each agglomerate in the population. This detailed popula-

tion balance model is coupled to the detailed chemistry with operator splitting, and solved using a stochastic technique.

The paper is structured as follows. After this introduction, the background to each of these three areas is described in turn. In the following section, the models developed for the gas phase chemistry and the detailed population balance are described. The results and discussion following this are again divided into the three areas: gas phase chemistry, surface chemistry, and the detail population balance. These are followed by the conclusions.

2 Background

2.1 Gas Phase Chemistry

Although the chloride process is a mature technology that has been used in industry since 1958, understanding of the gas-phase reactions of $TiCl_4$ oxidation remains incomplete [25].

The overall stoichiometry of this process is:

$$TiCl_4 + O_2 \rightarrow TiO_{2\,\text{(nanoparticles)}} + 2\,Cl_2. \tag{1}$$

There have been a few experimental investigations of the kinetics of the system: Pratsinis et al. [38] reported the overall oxidation kinetics of $TiCl_4$ at 700–1000 °C. The rate was found to be first order with respect to $TiCl_4$ and largely independent of O_2 concentration. This experimental work has been the basis for many theoretical studies of TiO_2 nanoparticle dynamics [33, 37, 42, 44]. However, these experiments were performed at temperatures much lower than those used in the industrial process. Extrapolation of kinetic data to this degree must be treated with caution.

The only oxychloride intermediate to have been observed directly is $TiOCl_2$ [20, 25] which suggests that it is likely to play an important role in the chemical mechanism.

A number of chemical mechanisms have been proposed [25, 38] but due to a lack of thermochemical data, no detailed simulations have previously been performed. Apart from the chlorides ($TiCl_y$), the only intermediate species with any published thermochemical data are TiOCl and $TiOCl_2$; these were estimated in 1963 with no explanation [8]. Our recent density functional theory (DFT) quantum calculations have elucidated the necessary thermochemical data [47]. With estimates of the rate expressions for elementary reactions, this enables development of a kinetic mechanism for the gas phase chemical reactions for the first time.

2.2 Surface Chemistry

TiO_2 is one of the most investigated metal oxide surfaces; details can be found in a recent comprehensive review article by Diebold [10]. Nevertheless, experimental investigations of the kinetics of the surface growth of rutile TiO_2 are scarce.

The rate of heterogenous TiO_2 surface growth was investigated at 400–850 °C [13] and this first order rate expression has been used in most modelling papers since [33, 37, 42, 44]. This extrapolation to higher temperatures should be treated with caution however, especially as a change in behaviour above 850 °C is reported [13]. A more detailed understanding of the elementary steps involved in the surface growth will help to develop a more reliable universal rate expression.

It is generally believed that after the seed is formed, $TiCl_4$ adsorbs and decomposes on the TiO_2 surface and subsequently molecular chlorine desorbs, leaving titanium atoms on the surface [37]. This titanium-covered surface is then oxidised by molecular oxygen and further $TiCl_4$ can adsorb and decompose. Bowker and co-workers investigated the kinetics of the reoxidation of reduced $TiO_2\{110\}$ [41], however, the full cycle of the growth is not yet fully understood. A scheme of the presumed surface growth from layer n to layer $n+1$ is given in Figure 1.

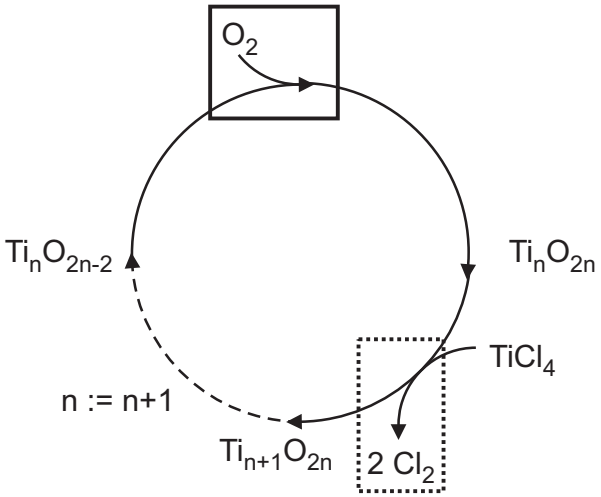

Figure 1 Surface Reaction Mechanism. Dotted box shows section studied recently [21]. Solid box shows section studied in this work.

Density functional theory (DFT) has proven to be a useful tool for the elucidation of reactions and diffusion processes on metals[23, 24, 29, 30] and metal oxides [6, 28, 39, 45]. The details of the elementary-step reaction mechanism for the $TiCl_4$ decomposition and chlorine formation are not fully understood. This motivated an investigation of the surface chemistry using plane-wave DFT. The diffusion and desorption of chlorine from a $TiO_2\{110\}$ surface (Figure 1, dotted box) was recently studied [21]. Figure 2, from Inderwildi and Kraft [21], shows that the adsorption of chlorine on a reduced $TiO_2\{110\}$ surface is strongly exothermic at all fractions of surface coverage: the desorption of chlorine from the reduced surface is energetically unfavourable at low temperatures. At high temperatures as in the flame synthesis of TiO_2, however, the chlorine will desorb (Le Chatelier).

The work presented here extends this investigation to include the adsorption of oxygen on the reduced $TiO_2\{110\}$ surface (Figure 1, solid box).

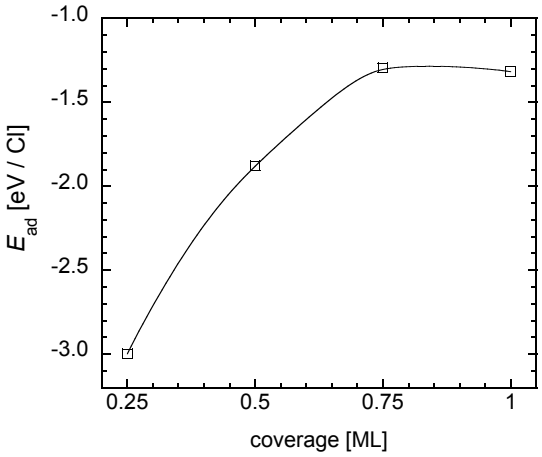

Figure 2 Chlorine adsorption on a reduced $TiO_2\{110\}$ surface, from Inderwildi and Kraft[21]

2.3 Population Balances

Considering the surface area and size of particles to be independent variables, non-spherical particle growth can be simulated using two-dimensional aerosol dynamics [50]. However, the non-linear integro-differential equation which describes the evolution of the two-dimensional particle size distribution (PSD) is difficult to solve directly; a summary of solution techniques is given in a review article by Kraft [27].

Simultaneous surface growth, coagulation, and sintering in this TiO_2 synthesis process have previously been modelled using both sectional[50] and moving sectional[42] 2-dimensional population balance models. Stochastic techniques have also been used to study this process [33], as well as to study the population balance of soot formation in carbon systems, such as premixed laminar flames [4]. Stochastic techniques do not suffer from the numerical diffusion inherent in sectional methods, and, unlike moment methods, are able to provide the full multivariate particle population density without additional model constraints.

Such a stochastic population balance solver has been successfully coupled to a deterministic solver for the gas-phase chemistry using operator splitting [7]. This coupling allows stochastic simulations to compete in an area only accessible before by sectional or moment methods.

The disadvantage of stochastic techniques for one-dimensional population balances is the additional computational time required for solution, though various algorithmic enhancements have been developed [35]. The major advantage of this stochastic technique is the ease with which additional particle properties can be tracked, with negligible increase in computational expense. This is used in the current work to develop an algorithm which enables the tracking of primary particles within each agglomerate particle, as will be described in section 3.2.

Stochastic algorithms offer the additional advantage of readily fitting into the standard

CFD framework, enabling the population balance to be elegantly coupled to the gas phase itself [46]. Typically the Particle In Cell (PIC) method is adopted, which treats the particles as a local source of momentum, kinetic energy and dissipation rate of turbulence. Although not all issues are resolved, it is hoped that in this way, stochastic methods will be able to bridge the gap between phases, and permit a complete description of the physics of TiO_2 production across the hierarchy of length scales to be obtained.

3 Model

This section describes the new developments in the three separate aspects of the current work towards a comprehensive model.

3.1 Gas Phase Chemistry

A detailed kinetic model consists of a list of intermediate species and the possible reactions between them. Each species must have thermochemical information, usually expressed in the form of polynomials for C_p, H, and S, and each reaction must have a forward rate expression, usually expressed in modified Arrhenius form, the backwards rate being calculated from the thermodynamic equilibrium constant.

The necessary thermochemical data for TiOCl, $TiOCl_2$, $TiOCl_3$, TiO_2Cl_2, TiO_2Cl_3, $Ti_2O_3Cl_3$, $Ti_2O_3Cl_2$, $Ti_2O_2Cl_3$, $Ti_3O_4Cl_4$, and $Ti_2O_2Cl_4$ were taken from recent quantum calculations [47]; those for $TiCl_3$, $TiCl_2$, and TiCl were taken from Hildenbrand[19]; and those for all other species were from the NASA database [16, 31].

Thermodynamic equilibrium calculations[47] can give clues to the chemical mechanism. The most stable intermediate with only one Ti atom is $TiOCl_2$, which has an equilibrium mole fraction orders of magnitude higher than any other monomer species, other than the titanium chlorides. The most stable dimer species is $Ti_2O_2Cl_4$. Gaseous TiO_2 is unstable and will exist in very low concentrations. The dimerisation of $TiOCl_2$ to form $Ti_2O_2Cl_4$ is therefore a more likely route towards the formation of TiO_2 nanoparticles than the dimerisation of gaseous TiO_2 molecules. The equilibrium calculations were used in this way to identify likely intermediate species and elementary steps in the reaction mechanism.

The elementary reactions of the species containing one Ti atom can be grouped into several categories. (i) Thermal decomposition which initiates the radical reaction chain, (ii) radical abstraction of Cl and disproportionation, (iii) oxidation, and (iv) dimerisation forming a $Ti_2O_xCl_y$ species.

Starting with a list of species, all the feasible reactions were devised manually using the above categories as prompts, eliminating reactions that violate spin conservation. If any of the reactions generate new species, these were added to the list, their thermochemistry was calculated, and new reactions that they could perform were devised.

Table 1 shows the reactions considered in the mechanism, along with the standard enthalpy of reaction at 298 K, and parameters for a modified Arrhenius rate expression for

the forward rate coefficient,

$$k_f = A \left(\frac{T}{1\ \mathrm{K}} \right)^n \exp\left(\frac{E_a}{RT} \right), \tag{2}$$

where T is the temperature in Kelvin.

Table 1: *Reaction mechanism equations*

No	Reaction	ΔH°_{298K} [a]	A [b]	n	E_a [a]	Ref.
Thermal Decomposition						
R1	$TiCl_4$ + M ⇌ $TiCl_3$ + Cl + M	387	5.40×10^{18}	0	336	[18]
R2	$TiCl_3$ + M ⇌ $TiCl_2$ + Cl + M	422	7.70×10^{18}	0	387	[18]
R3	$TiCl_2$ + M ⇌ TiCl + Cl + M	507	3.20×10^{17}	0	511	[43]
R4	Ti + Cl ⇌ TiCl	−405	1.00×10^{13}	0	0	
R5	$TiCl_2$ + Cl_2 ⇌ $TiCl_4$	−567	1.00×10^{13}	0	0	
R6	TiCl + Cl_2 ⇌ $TiCl_3$	−687	1.00×10^{13}	0	0	
Abstraction and Disproportionation						
R7	$TiCl_3$ + Cl_2 ⇌ $TiCl_4$ + Cl	−144	1.00×10^{13}	0	0	
R8	$TiCl_2$ + Cl_2 ⇌ $TiCl_3$ + Cl	−180	1.00×10^{13}	0	0	
R9	TiCl + Cl_2 ⇌ $TiCl_2$ + Cl	−265	1.00×10^{13}	0	0	
R10	Ti + Cl_2 ⇌ TiCl + Cl	−162	1.00×10^{13}	0	0	
R11	$TiCl_4$ + TiCl ⇌ $TiCl_3$ + $TiCl_2$	−121	1.00×10^{13}	0	0	
R12	$TiCl_4$ + Ti ⇌ $TiCl_3$ + TiCl	−18	1.00×10^{13}	0	0	
R13	$TiCl_2$ + TiCl ⇌ $TiCl_3$ + Ti	−17	1.00×10^{13}	0	0	
R14	2 TiCl ⇌ $TiCl_2$ + Ti	−103	1.00×10^{13}	0	0	
R15	Cl_2 + TiO_2Cl_2 ⇌ Cl + TiO_2Cl_3	−95	1.00×10^{13}	0	0	
R16	Cl_2 + $Ti_2O_2Cl_3$ ⇌ Cl + $Ti_2O_2Cl_4$	−174	1.00×10^{13}	0	0	
R17	2 $TiCl_3$ ⇌ $TiCl_2$ + $TiCl_4$	35	9.60×10^{12}	0	35	[18] [d]
R18	$TiCl_3$ + TiCl ⇌ 2 $TiCl_2$	−85	1.00×10^{13}	0	0	
Oxidation						
R19	$TiCl_3$ + O_2 ⇌ TiO_2Cl_3	−277	1.00×10^{13}	0	0	
R20	$TiOCl_3$ + ClO ⇌ TiO_2Cl_3 + Cl	−115	1.00×10^{13}	0	0	
R21	TiO_2Cl_3 + $TiCl_3$ ⇌ 2 $TiOCl_3$	−7	1.00×10^{13}	0	0	
R22	$TiOCl_2$ + Cl ⇌ $TiOCl_3$	−162	1.00×10^{13}	0	0	
R23	$TiOCl_3$ + O ⇌ TiO_2Cl_3	−384	1.00×10^{13}	0	0	
R24	TiO_2Cl_2 + Cl ⇌ TiO_2Cl_3	−337	1.00×10^{13}	0	0	
R25	TiO_2Cl_2 + Cl ⇌ $TiCl_3$ + O_2	−61	1.00×10^{13}	0	0	
R26	$TiOCl_3$ + O ⇌ $TiCl_3$ + O_2	−108	1.00×10^{13}	0	0	
R27	$TiCl_2$ + O_2 ⇌ $TiOCl_2$ + O	−152	1.00×10^{13}	0	0	
R28	TiO_2Cl_2 + O ⇌ $TiOCl_2$ + O_2	−289	1.00×10^{13}	0	0	
R29	$TiCl_3$ + ClO ⇌ $TiCl_4$ + O	−118	1.00×10^{13}	0	0	
R30	$TiCl_2$ + ClO ⇌ $TiCl_3$ + O	−153	1.00×10^{13}	0	0	
R31	TiCl + ClO ⇌ $TiCl_2$ + O	−239	1.00×10^{13}	0	0	
R32	Ti + ClO ⇌ TiCl + O	−136	1.00×10^{13}	0	0	
R33	$TiCl_3$ + O ⇌ $TiOCl_2$ + Cl	−228	1.00×10^{13}	0	0	

[a] kJ mol^{-1} [b] cm^3 mol^{-1} s^{-1} [c] cm^6 mol^{-2} s^{-1} [d] estimate

Table 1: *Reaction mechanism equations – Continued.*

No	Reaction	ΔH°_{298K} [a]	A [b]	n	E_a [a]	Ref.
R34	$TiCl_3 + Cl_2O \rightleftharpoons TiCl_4 + ClO$	−243	1.00×10^{13}	0	0	
R35	$TiCl_3 + ClO \rightleftharpoons TiOCl_3 + Cl$	−122	1.00×10^{13}	0	0	
R36	$TiO_2Cl_2 + Cl \rightleftharpoons TiOCl_2 + ClO$	−60	1.00×10^{13}	0	0	
Cl/O Chemistry						
R37	$O + O_2 + M \rightleftharpoons O_3 + M$	−107	1.84×10^{21} [c]	-2.8	0	[2]
R38	$ClOO + M \rightarrow Cl + O_2 + M$	24	1.69×10^{14}	0	15.13	[2]
R39	$Cl + O_2 + M \rightarrow ClOO + M$	−24	8.68×10^{21} [c]	-2.9	0	[2]
R40	$Cl + O_3 \rightleftharpoons ClO + O_2$	−161	1.75×10^{13}	0	2.18	[3]
R41	$Cl_2O + Cl \rightleftharpoons Cl_2 + ClO$	−99	3.73×10^{13}	0	-1.09	[3]
R42	$Cl + O_2 \rightleftharpoons ClO + O$	229	8.79×10^{14}	0	230.5	[5]
R43	$O + Cl_2 \rightleftharpoons ClO + Cl$	−26	4.46×10^{12}	0	13.73	[49]
R44	$2\,Cl + M \rightleftharpoons Cl_2 + M$	−243	2.23×10^{14} [c]	0	-7.53	[5]
Dimerisation and dimer reactions						
R45	$2\,TiOCl_2 \rightleftharpoons Ti_2O_2Cl_4$	−356	1.00×10^{13}	0	0	
R46	$TiO_2Cl_2 + TiCl_3 \rightleftharpoons Ti_2O_2Cl_4 + Cl$	−375	1.00×10^{13}	0	0	
R47	$TiO_2Cl_2 + TiOCl_2 \rightleftharpoons Ti_2O_3Cl_3 + Cl$	−141	1.00×10^{13}	0	0	
R48	$TiOCl_2 + TiOCl_3 \rightleftharpoons Ti_2O_2Cl_4 + Cl$	−194	1.00×10^{13}	0	0	
R49	$Ti_2O_3Cl_3 + TiOCl_2 \rightleftharpoons Ti_3O_4Cl_4 + Cl$	−164	1.00×10^{13}	0	0	
R50	$Ti_2O_3Cl_2 + Cl \rightleftharpoons Ti_2O_3Cl_3$	−208	1.00×10^{13}	0	0	
R51	$Ti_2O_2Cl_3 + TiCl_4 \rightleftharpoons Ti_2O_2Cl_4 + TiCl_3$	−29	1.00×10^{13}	0	0	

[a] kJ mol^{-1} [b] cm^3 mol^{-1} s^{-1} [c] cm^6 mol^{-2} s^{-1} [d] estimate

The rate parameters for the initiating reactions (R1 and R2 in Table 1) were taken from high temperature shock tube experiments by Herzler and Roth[18] which agree with values from a theoretical study by Teyssandier and Allendorf [43]. This study was also the source of the parameters for reaction R3 [43]. Oxygen-chlorine chemistry in reactions R37–R44 was taken from the literature. [2, 3, 5, 49]

The remaining rate parameters were estimated as having a pre-exponential factor, A, given by the collision limit 1×10^{13} mol cm^{-3} s^{-1}, and the activation energy, E_a, in the exothermic direction was taken to be zero. For this reason all the reactions with estimated parameters are listed in the exothermic direction in Table 1.

This barrier-less estimate provides an approximate upper limit for the reaction rates. For the radical combination reactions this is a reasonable estimate. Work is underway to calculate the transition states of key reactions using quantum calculations, to determine more accurate rate parameters. Some reactions which proceed via activated intermediates will probably be significantly slowed by fall-off, and some chemically-activated product channels will open. The effect of this will be estimated in future work, but it is expected to affect reactions in which two species combine to form one species in the exothermic direction (R19, R22, R23, R24, R45, R50).

Our current mechanism includes 51 elementary reactions and oxidises $TiCl_4$ to form a

stable $Ti_2O_xCl_y$ 'dimer' species, which we believe lies on the path towards TiO_2 nanoparticles. We shall continue this work to improve our rate estimates and extend the mechanism towards the stage where it can be directly coupled to the particle model with greater confidence.

3.2 Population Balance Modelling

To simulate the comprehensive model of chemistry and particle dynamics, the previous surface volume model[36] was extended to account for particle structure and coupled to the gas phase chemistry simulation using operator splitting [7]. The gas-phase chemistry is solved deterministically using a standard ODE solver. The rest of this section will describe the population balance model used to describe the particle population.

3.2.1 Particle description

The current work extends a previous two-dimensional surface–volume model [36], which provided some shape information about the particles and allowed particle sintering to be modelled. Using the surface–volume model for this system, a stochastic particle would be defined in the solver as a vector of TiO_2 monomer count and surface area; all other particle properties, and hence particle process rates, would be calculated from these. In this extension to the model, the sizes of the primary particles within each agglomerate particle are also tracked. An agglomerate particle in the current population balance is therefore described by the number of TiO_2 monomers in the particle, M, the surface area of the particle, A, and the number of TiO_2 monomers in each of the primary particles that make up the agglomerate, $\vec{m} = (m_1, m_2, m_3, \ldots)$. For each primary particle the volume is found by multiplying the monomer count by the molar volume of rutile, and the surface area by assuming the primary particles are spherical.

For a simulation in which the highest number of primaries in a single agglomerate reaches N, the population balance effectively has $(N + 2 - 1)$ dimensions (the -1 is because $\sum_{i=1}^{N} m_i = M$). This expansion of the population balance to $N+1$ dimensions ($N \sim 10^2$) rules out the use of sectional methods, in which the computation times scale exponentially with the number of dimensions. (A 2-D sectional simulation by Muhlenweg *et al.* for a similar system took about 112 days on a 300 MHz alpha workstation [34].) The stochastic particle method used to solve the population balance makes it computationally cheap to track many internal co-ordinates within the population. This Linear Process Deferment Algorithm (LPDA) used here is explained by Patterson *et al.*[35]. Like a Direct Simulation Monte Carlo algorithm, it requires only a set of rules for creating and modifying the particles, and their associated rates. We define these in sections 3.2.2 to 3.2.5.

3.2.2 Inception.

At some point in the simulated growth mechanism the collision and merging of two molecules to form a third will necessarily be treated as a particle coagulation event rather

than a gas phase chemical reaction. Because the particle model does not include a breakage term, this coagulation is treated as irreversible, unlike a gas phase chemical reaction.

In the current study, the collision of any two molecules containing two or more Ti atoms each is treated as a particle inception. The rate of these events is dependent on the concentration of the species involved, and is estimated according to collision theory, with the collision diameter estimated from the DFT results to be 0.65 nm (the diameter of the sphere with a volume equivalent to that occupied by the Connolly surface of $Ti_2O_2Cl_4$).

Studies of thermodynamic equilibrium composition based on the calculated thermochemistry [47] suggest that at temperatures of ¿ 600 K the critical nucleus size, above which molecules (or particles) prefer to grow than to shrink, probably contains at least five titanium atoms. In the present model, the transition from reversible gas phase reaction to irreversible particle coagulation is premature, so the nucleation rate computed using this model is expected to be an overestimate. However, the present approach is a significant improvement over previous studies of this system which have treated the unstable triatomic molecule TiO_2 as a nucleated particle [33, 37, 42, 44].

When a particle is first incepted from the gas phase, it is assumed to be spherical, and its primary particle list is initiated with one entry whose size (monomer count) equals that of the incepted particle.

For example, the inception reaction

$$Ti_2O_2Cl_4 + Ti_2O_3Cl_2 \rightarrow \underbrace{(TiO_2)_4}_{\text{particle}} + 3Cl_2 - 1.5O_2 \tag{3}$$

would create a particle with the properties

$$M = \text{number of Ti atoms} = 4 \tag{4}$$

$$A = \pi^{1/3}\left(\frac{6M}{\rho}\right)^{2/3} \tag{5}$$

$$m_1 = M \tag{6}$$

where ρ is the molar density of bulk rutile.

3.2.3 Surface Growth.

Although progress is being made towards a better understanding of the surface chemistry of this system, due to a lack of kinetic data the current population balance uses the commonly used[33, 37, 42, 44] one-step expression given by Ghoshtagore [13].

$$\frac{dM}{dt} = A[TiCl_4]4.9 \times 10^3 \text{ cm s}^{-1} \exp\left(\frac{-74.8 \text{ kJ mol}^{-1}}{k_B T}\right) \tag{7}$$

where A is the surface area of the particle, $[TiCl_4]$ is the concentration of $TiCl_4$ in the gas phase, T is the temperature and k_B is Boltzmann's constant.

When chemical reactions on the surface increase the number of TiO_2 monomer units in a particle by a number ΔM, the volume of the particle increases by $\Delta M/\rho$, where ρ is the

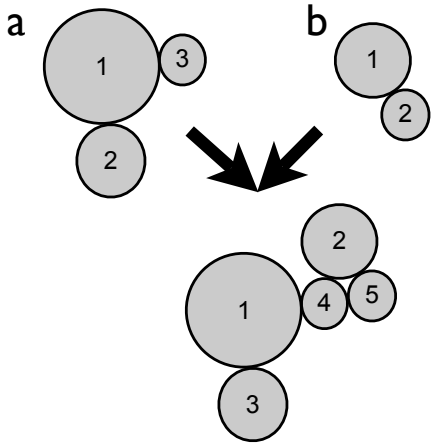

Figure 3 Coagulation of particles a and b.

molar density of bulk rutile. For non-spherical particles, the effect this surface growth has on the surface area of the particle (dA/dM and thus dA/dt) is less obvious. To calculate this we use the radius of curvature method explained by Patterson and Kraft [36]. This model causes surface reactions to increase the sphericity of particles as suggested by TEM images of soot particles.

When surface growth is determined to have added a certain number (ΔM) of monomer units to a particle, these are distributed amongst the constituent primary particles randomly, with probabilities proportional to their spherical surface areas ($p_i \propto m_i^{2/3}$).

3.2.4 Coagulation.

The rates of collisions between particles of different sizes and shapes is determined by the coagulation kernel, in this case a function of M and A. Different coagulation kernels are appropriate in different conditions (particle size and gas pressure); see Singh et al. [40] for details. These coagulation kernels are also used to model the particle inception processes.

When two particles coagulate the monomer count and surface area are conserved, and the lists of constituent primary particles are appended to one another. For example, when two particles a and b, with properties $(M_a, A_a, m_{a1}, m_{a2}, m_{a3})$ and $(M_b, A_b, m_{b1}, m_{b2})$, coagulate as illustrated in Figure 3, the resulting agglomerate particle will be given by

$$\begin{aligned} M &= M_a + M_b \\ A &= A_a + A_b \\ m_1 &= m_{a1} \\ m_2 &= m_{b1} \\ m_3 &= m_{a2} \\ m_4 &= m_{a3} \\ m_5 &= m_{b2}. \end{aligned}$$

3.2.5 Sintering.

To model sintering we follow the approach of Xiong and Pratsinis[50] and assume that the excess agglomerate surface area, over that of a spherical particle with the same mass, decays exponentially.

$$\frac{dA}{dt} = -\frac{1}{\tau_f}\left(A - \pi^{1/3}\left(\frac{6M}{\rho}\right)^{2/3}\right) \tag{8}$$

As in previous works [33, 50], the characteristic time was given by the expression for TiO_2 particles sintering through grain boundary diffusion obtained by Kobata *et al.* [26]:

$$\tau_f = 7.4 \times 10^8 \mathrm{K}^{-1}\, T\, d_p^4 \exp\left(\frac{3.1 \times 10^4 \mathrm{K}}{T}\right) \tag{9}$$

where $d_p = 6M/\rho A$ is a measure of average primary particle diameter.

As specified above, the surface area of an aggregate particle in this simulation is tracked independently and determined by the sintering and surface growth models. The list of primary particles is updated to match this surface area value according to the following scheme, inspired by Ostwald ripening:

1. If the sum of the primary particle surface areas exceeds the required aggregate surface area, then go to step 2, otherwise end.
2. Select the smallest primary particle.
3. Remove this primary particle from the list, noting its monomer count (size).
4. Redistribute the monomers across the other primary particles randomly, with probabilities in proportion to their surface areas.
5. Recalculate the surface areas of the primary particles.
6. Go to step 1.

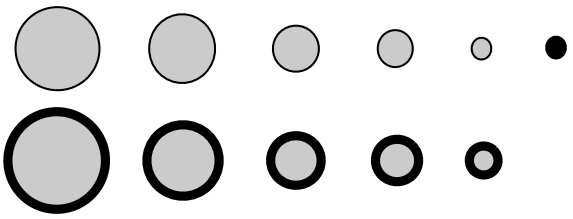

Figure 4 Primary particles before (top) and after (bottom) sintering.

3.2.6 Shape estimation

In order to generate shape information, to aid visualisation of the particles, the positions of the primary particles within a particle are generated in a post-processing step: The primary particles are shuffled into a random order and one of them is placed at the origin. The remaining primary particles are placed according to this algorithm: (1) The centre of mass is found for the primary particles that have already been placed. (2) A vector from this centre of mass is chosen in a random direction. (3) The next primary particle is placed on this vector in a position where it just touches an already placed primary particle.

4 Results and Discussion

4.1 Gas Phase Chemistry

The chemical mechanism, thermochemistry, and rate parameters described above were used to simulate a zero dimensional batch reactor at constant temperature and pressure (1500 K, 3×10^5 Pa) with an initial mixture of 50 mol% $TiCl_4$ in O_2. These conditions are close to those in a typical industrial reactor [1, 11]. The simulation was carried out using Cantera [15]. The time-evolutions of the species mole fractions over the first 10 ms are shown in Figures 5 and 6. The overall process is the conversion of $TiCl_4$ into the dimer species $Ti_2O_2Cl_4$ (Figure 5). Figure 6 is plotted on a logarithmic scale and shows the details of the reactive intermediates.

The main reaction sequence (Fig. 7) begins with the formation of $TiCl_3$ radicals from $TiCl_4$, primarily via radical abstraction (the reverse of reaction R7 in Table 1, hereinafter denoted R7'),

$$TiCl_4 + Cl \rightleftharpoons TiCl_3 + Cl_2, \tag{R7'}$$

but also by pressure-dependent thermal decomposition (R1 in the forwards direction):

$$TiCl_4 + M \rightleftharpoons TiCl_3 + Cl + M. \tag{R1}$$

These $TiCl_3$ radicals are then oxidised to give $TiOCl_3$, some directly,

$$TiCl_3 + ClO \rightleftharpoons TiOCl_3 + Cl, \tag{R35}$$

but the majority via TiO_2Cl_3:

$$TiCl_3 + O_2 \rightleftharpoons TiO_2Cl_3 \tag{R19}$$

$$TiO_2Cl_3 + Cl \rightleftharpoons TiOCl_3 + ClO \tag{R20'}$$

$$TiO_2Cl_3 + TiCl_3 \rightleftharpoons 2\ TiOCl_3. \tag{R21}$$

$TiOCl_3$ reacts to form the more stable intermediate $TiOCl_2$ via

$$TiOCl_3 \rightleftharpoons TiOCl_2 + Cl. \tag{R22'}$$

Once sufficient $TiOCl_2$ has formed, it dimerises to form $Ti_2O_2Cl_4$:

$$2\ TiOCl_2 \rightleftharpoons Ti_2O_2Cl_4. \tag{R45}$$

This is a first step towards a nanoparticle containing thousands of TiO_2 units.

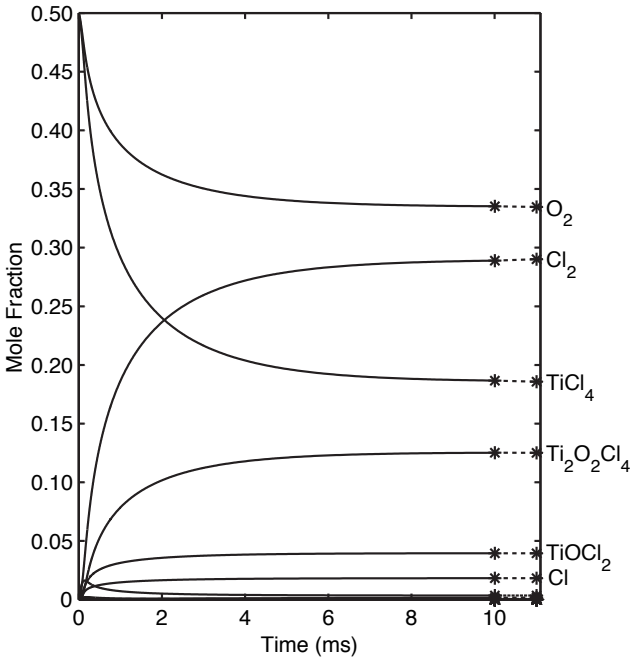

Figure 5 Species mole fractions versus time. Initial composition was 50 mol% $TiCl_4$ in O_2 at time$= 0$. Constant T=1500 K, P=3×10^5 Pa. The dashed line to the final star shows the mole fraction at thermodynamic equilibrium.

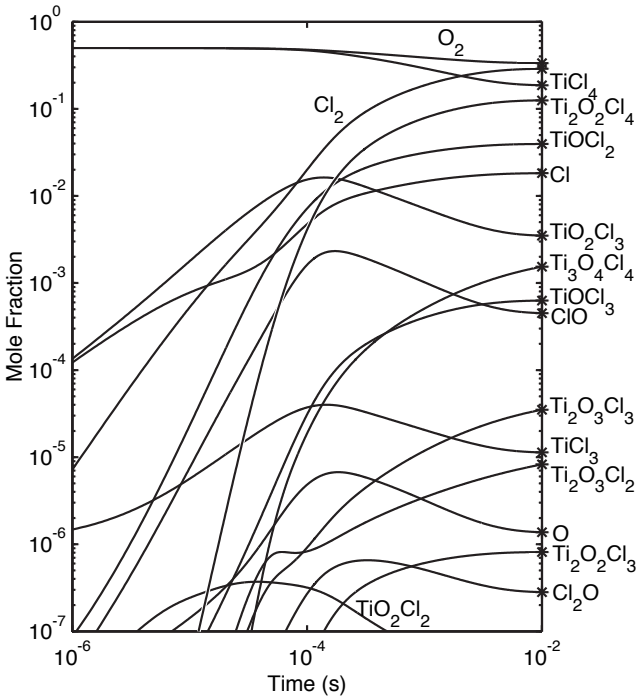

Figure 6 Species mole fractions (logarithmic) versus time (logarithmic). Starting composition was 50 mol% $TiCl_4$ in O_2 at time$= 0$. Constant T=1500 K, P=3×10^5 Pa.

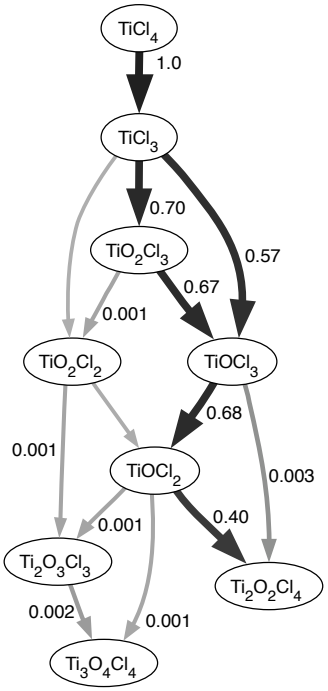

Figure 7 The main reaction paths showing relative net flux of species at 72 μs, by which time 1 % of the $Ti_2O_2Cl_4$ has been formed.

Table 2 Kinetic Sensitivity Analysis

No.	Reaction	Sensitivity[a]
R21	$TiO_2Cl_3 + TiCl_3 \rightleftharpoons 2\ TiOCl_3$	0.24
R1	$TiCl_4 + M \rightleftharpoons TiCl_3 + Cl + M$	0.05
R35	$TiCl_3 + ClO \rightleftharpoons TiOCl_3 + Cl$	0.05
R7	$TiCl_3 + Cl_2 \rightleftharpoons TiCl_4 + Cl$	0.05
R19	$TiCl_3 + O_2 \rightleftharpoons TiO_2Cl_3$	0.007
R47	$TiO_2Cl_2 + TiOCl_2 \rightleftharpoons Ti_2O_3Cl_3 + Cl$	−0.007
R20	$TiOCl_3 + ClO \rightleftharpoons TiO_2Cl_3 + Cl$	0.005

[a] Sensitivity = $\Delta\left(\log(x_{1\text{ms}})\right) / \Delta\left(\log(A)\right)$ where $x_{1\text{ms}}$ is the mole fraction of $Ti_2O_2Cl_4$ at $t = 1$ ms and A is the pre-exponential factor for the reaction rate (see Eqn. 2).

4.1.1 Sensitivity Analysis

The sensitivity of the overall reaction rate was investigated with respect to changes in both the individual rate coefficients of each reaction, and the thermochemistry of each species. A 1:1 molar ratio of O_2 and $TiCl_4$ was simulated at 3×10^5 Pa and 1500 K and the mole fraction of the dimer $Ti_2O_2Cl_4$ at $t = 1$ ms was noted.

Increasing the rate of reaction R21 (both forward and reverse, i.e., fixed thermochemistry) by a factor of three increases the mole fraction of the dimer after 1 ms by 30%, see Table 2. A few other rate constants also noticeably affect the dimer formation kinetics. However, in general the kinetics are relatively insensitive to the assumed rate constants.

The kinetics are naturally sensitive to the enthalpies of formation of $TiCl_4$, O_2, and Cl_2, but fortunately all of these are very well established. Of the species with poorly established thermochemistry, the kinetics are most sensitive to the enthalpies of $TiCl_3$ and the dimer $Ti_2O_2Cl_4$; making either species 50 kJ mol^{-1} less stable decreases the concentration of $Ti_2O_2Cl_4$ after 1 ms by about a factor of 5. The other Ti-containing species have a much weaker effect on the predicted kinetics (see Fig. 8).

Hildenbrand [19] has persuasively argued that the NASA and JANAF [8, 32] enthalpies for $TiCl_3$ are inaccurate by about 42 kJ/mole at 298 K; using the JANAF estimate for $TiCl_3$ rather than Hildenbrand's estimate increases the overall reaction rate by about 12%. Our DFT-based estimate of the enthalpy of formation of $Ti_2O_2Cl_4$ is unfortunately the only value in the literature; because there is no reliable reference species available on which to base an isodesmic reaction, 50 kJ mol^{-1} is a reasonable estimate of the uncertainty.

4.2 Surface Chemistry

In addition to the investigation of the seed formation in the gas phase using orbital centred DFT, plane-wave DFT calculations were applied to study the growth process of rutile TiO_2 surfaces. Details of the calculation methods are given by Inderwildi and Kraft [21]. Two stages of the surface growth of TiO_2 have now been studied. Firstly, the diffusion and

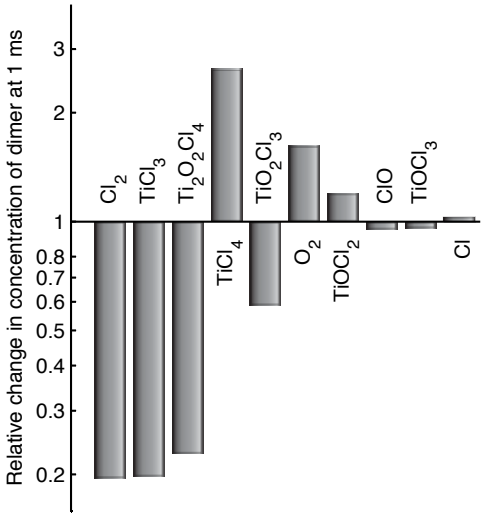

Figure 8 Sensitivity of the concentration of $Ti_2O_2Cl_4$ after 1 ms to a 50 kJ mol^{-1} increase in enthalpy of formation of each species. Constant T=1500 K, P=3×10^5 Pa.

desorption of chlorine, formed by decomposition of $TiCl_4$, from a $TiO_2\{110\}$ surface was studied [21]. In this work, the adsorption of oxygen on reduced $TiO_2\{110\}$ was also studied.

Figure 9 shows the average adsorption energy of oxygen on a reduced $TiO_2\{110\}$ surface, as function of the surface coverage. Oxidation of the reduced $TiO_2\{110\}$ is initially energetically very favourable, the formation of a stoichiometric surface is still favourable (Coverage = 0.5 ML), while the full oxidation is thermoneutral. This oxidation of reduced $TiO_2\{110\}$ will be a crucial step in the synthesis of rutile TiO_2, since decomposition of $TiCl_4$ or oxychloride species will be rather fast, while the results presented here indicate that the oxidation, especially the full oxidation, is presumably slow compared to the $TiCl_4$ decomposition since the full oxidation is overall thermoneutral (BEP relation) [22].

We believe this work will lead to an improved understanding of the surface growth mechanism that can be used directly in population balance modelling.

4.3 Coupled Gas Phase and Particle Simulation

The combined simulation coupling the gas phase kinetic model to the particle dynamics model was used to simulate the tubular flow reactor described by Pratsinis [38]. Figure 10 shows the evolution of the primary particle size distribution from a simulation of a plug flow reactor at constant temperature of 800 °C starting with a feed of 0.2 mol% $TiCl_4$ and 1 mol% O_2 in Argon. The simulation used the developmental gas phase mechanism from section 3.1 with surface chemistry from Ghoshtagore[13] coupled to the population balance described in section 3.2. To give an indication of the possible shapes of the agglomerate particles, Figure 11 shows TEM-style images of the first particle from the same simulation. The geometric information was generated as described above.

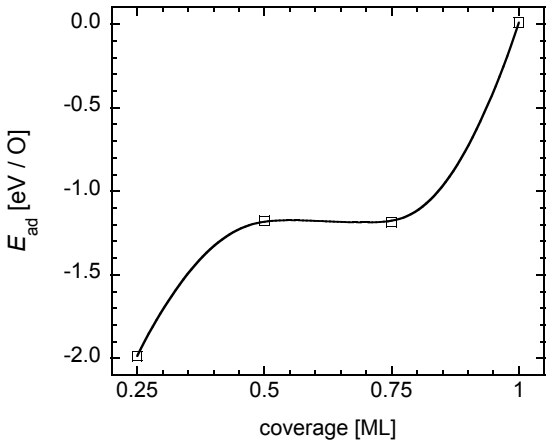

Figure 9 Oxygen adsorption on a reduced $TiO_2\{110\}$ surface

Because the kinetic model is thought to be incomplete and has not had any free parameters adjusted to fit experimental data, the time-scales on the simulation are likely to be inaccurate. According to the simulation, at 0.5 seconds most of the particles are newly incepted and so the primary particle size distribution is very narrow and the average diameter is very small: the particles are essentially all $(TiO_2)_4$ molecules. After 1 second the particles have had opportunities to coagulate and form agglomerates. Those primary particles which coagulated early will have also had sufficient time to sinter together and to grow through surface reactions. However, there are still many new primary particles nucleating from the gas phase at this stage. The primary particle size distribution is seen to grow and broaden, both within the population (Figure 10) and within individual particles (Figure 11). Although the flow time through the experimental reactor was $\sim$1 second, the simulation was continued until 10 seconds. After 5 seconds the average primary particle diameter has increased to about 50 nm. The absolute width of the distribution is similar to that at 1 second, so the relative width is much narrower, leading to much more mono-disperse appearance as seen in the TEM-style images. This trend continues up to 10 seconds, by which time the primary particles have reached nearly 80 nm diameter.

The simulation was repeated for conditions nearer those of an industrial reactor: an equimolar ratio of $TiCl_4$ and O_2 fed to a plug flow reactor at 3×10^5 Pa pressure, with a temperature profile constant at 1500 K for 100 ms, falling linearly to 1000 K over the next 100 ms.

The very high concentration of reactants and high temperature causes a large burst of particle inception, peaking at 0.1 ms. Particles from 0.1 and 0.2 ms are shown in Figure 12. Within 0.4 ms, 90 % of the $TiCl_4$ is consumed and the inception rate has dropped to 0.5 % of its peak value. This rapid burst of particle inception near the beginning of the reactor leads to a very narrow primary particle size distribution (Figure 13). After 200 ms most primary particles in the simulation have a diameter of about 45 nm. Pigmentary titania from industrial reactors, after a further 10 seconds in a plug flow cooler, typically has an average primary particle size of 250 nm [11]. Given the approximations in the current set of sub-models, this level of agreement is encouraging.

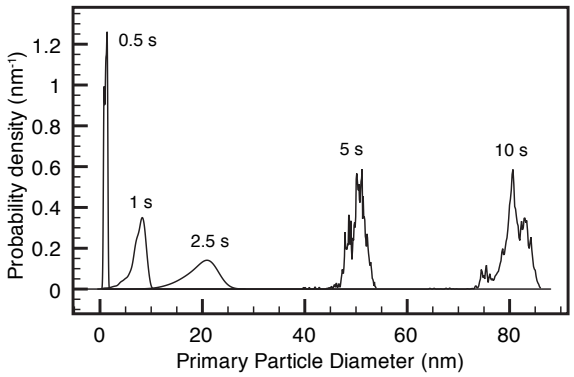

Figure 10 Primary particle size distribution (mass weighted) after various times at 800 °C.

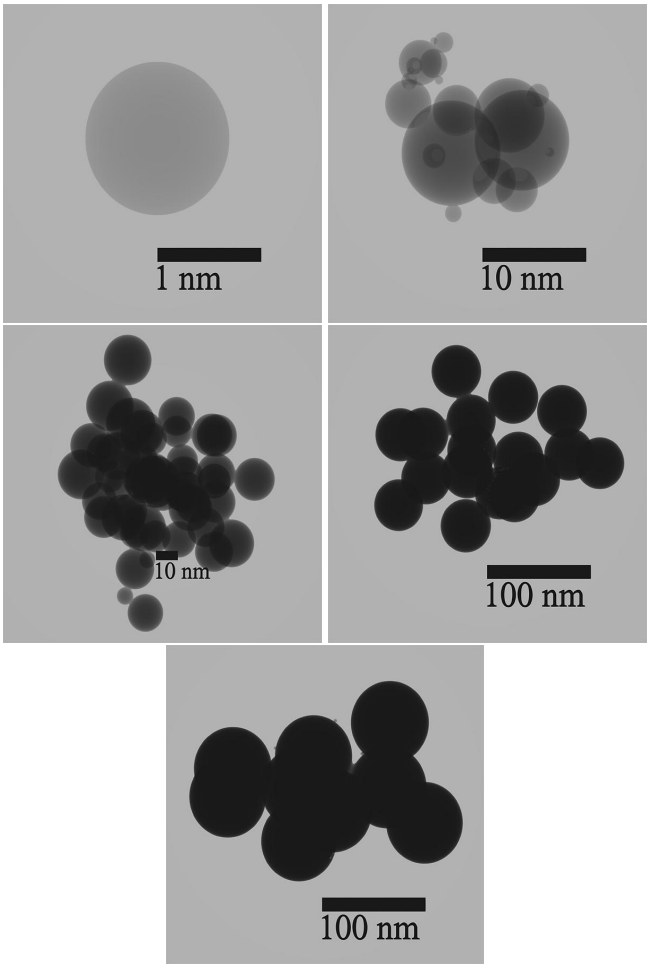

Figure 11 TEM-style images of the oldest particle in the simulation after 0.5, 1, 2.5, 5 and 10 seconds at 800 °C.

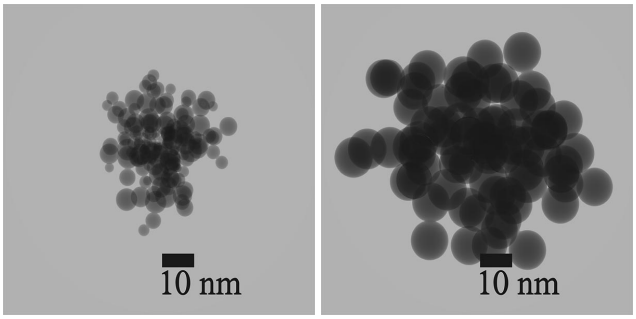

Figure 12 TEM-style images of the oldest particle after 0.1 and 0.2 ms in the industrial reactor simulation.

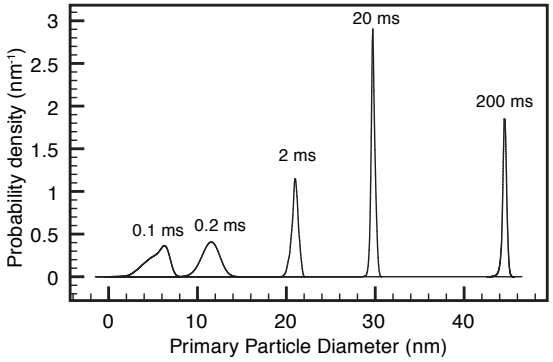

Figure 13 Primary particle size distributions (mass weighted) at various times in the industrial reactor simulation.

5 Conclusions

Significant progress has been made from first principles towards a comprehensive model of the combustion of $TiCl_4$ to form TiO_2 particles, one of the largest volume processes using combustion synthesis.

Using recently published thermochemical data for the $TiCl_xO_y$ intermediates [47], the present work demonstrates for the first time that it is possible to construct sensible, thermodynamically consistent kinetic models for this important process. As a start, a rough kinetic model was constructed using the new thermochemistry; this model was found to be at least qualitatively correct, rapidly converting $TiCl_4$ to oxygen-containing dimers. Additional work is required to detail the subsequent chemistry of the dimers and trimers. The model predictions are fortunately not sensitive to the assumed rate parameters, though certainly the model would be improved by the inclusion of fall-off effects. The model predictions are fairly sensitive to the thermochemistry of the $TiCl_3$ and TiO_2Cl_2 intermediates.

Plane-wave DFT investigations of the oxygen and chlorine adsorption on rutile $TiO_2\{110\}$ showed that the oxidation of the reduced $TiO_2\{110\}$ surface might be the rate determining step in the formation of bigger nanoparticles. Firstly because the barrier for the adsorption of oxygen is the highest, and secondly because the presented study indicates that oxygen "pushes" the chlorine into a position from which it can desorb more easily. These findings lead towards a better understanding of the surface mechanism, which will in turn lead to an improved kinetic model for surface reactions in this system.

A new multivariate population balance model was devised in which, in addition to surface area and volume, the size of every primary particle within each agglomerate particle in the population is tracked. The population balance model was solved using a stochastic particle algorithm coupled to the detailed gas phase chemical mechanism using an operator splitting technique. This new population balance model allows the primary particle size distribution to be followed explicitly, and simple post-processing generates spatial information, presented here in the form of TEM-style images.

By coupling a new detailed kinetic model, generated from quantum chemical calculations, to a new population balance model with primary particle tracking, the current work demonstrates the feasibility of using first-principles modelling to tackle industrially important chemical engineering questions.

Recent advances in population balance modelling are such that further work on developing a kinetic model for the chemical mechanism could now have a real impact on the ability to predict important product properties, such as paint opacity; theoretical work towards such a kinetic model would be greatly assisted by new experimental data recorded under well defined conditions.

Acknowledgements

The authors would like to thank the EPSRC and Tioxide Europe Limited for the financial support of RHW through an Industrial CASE studentship. Additional financial support

from the EPSRC grant number EP-E01724X-1 and the US National Science Foundation is gratefully acknowledged. WHG thanks Churchill College for a Bye-Fellowship which greatly facilitated this collaboration.

References

[1] A. Allen and G. R. Evers. TiO_2 manufacturing process, us patent 5201949. US Patent, 1992.

[2] R. Atkinson, D. L. Baulch, R. A. Cox, R. F. Hampson, J. A. Kerr, M. J. Rossi, and J. Troe. Evaluated kinetic and photochemical data for atmospheric chemistry: Supplement VI - IUPAC subcommittee on gas kinetic data evaluation for atmospheric chemistry. *J. Phys. Chem. Ref. Data*, 26:1329–1499, 1997.

[3] R. Atkinson, D. L. Baulch, R. A. Cox, R. F. Hampson, J. A. Kerr, M. J. Rossi, and J. Troe. Summary of evaluated kinetic and photochemical data for atmospheric chemistry, December 2001. URL `www.iupac-kinetic.ch.cam.ac.uk`.

[4] M. Balthasar and M. Kraft. A stochastic approach to calculate the particle size distribution function of soot particles in laminar premixed flames. *Combust. Flame*, 133:289–298, 2003. doi:10.1016/S0010-2180(03)00003-8.

[5] D. L. Baulch, J. Duxbury, S. J. Grant, and D. C. Montague. Evaluated kinetic data for high temperature reactions. volume 4 homogeneous gas phase reactions of halogen- and cyanide- containing species. *J. Phys. Chem. Ref. Data*, 10(Suppl. 1):1–721, 1981.

[6] P. Broqvist, I. Panas, and H. Grönbeck. Toward a realistic description of NO_x storage in BaO: The aspect of $BaCO_3$. *J. Phys. Chem. B*, 109(19):9613–9621, 2005. doi:10.1021/jp050384l.

[7] M. Celnik, R. Patterson, M. Kraft, and W. Wagner. Coupling a stochastic soot population balance to gas-phase chemistry using operator splitting. *Combust. Flame*, 148 (3):158–176, 2007. doi:10.1016/j.combustflame.2006.10.007.

[8] M. W. Chase Jr. NIST-JANAF thermochemical tables, fourth edition. *J. Phys. Chem. Ref. Data*, Monograph 9, 1998.

[9] J. C. Deberry, M. Robinson, M. Pomponi, A. J. Beach, Y. Xiong, and K. Akhtar. Controlled vapor phase oxidation of titanium tetrachloride to manufacture titanium dioxide, us patent 6387347. US Patent, 2002.

[10] U. Diebold. The surface science of titanium dioxide. *Surf. Sci. Rep.*, 48(5-8):53–229, 2003. doi:10.1016/S0167-5729(02)00100-0.

[11] J. Edwards (Huntsman Pigments,Tioxide Europe Limited). Personal communication, 2007.

[12] J. Emsley. *Molecules at an Exhibition*. Oxford University Press, 1999.

[13] R. N. Ghoshtagore. Mechanism of heterogeneous deposition of thin film rutile. *J. Electrochem. Soc.*, 117:529–534, 1970. doi:10.1149/1.2407561.

[14] R. A. Gonzalez, C. D. Musick, and J. N. Tilton. Process for controlling agglomeration in the manufacture of TiO_2, us patent 5508015. US Patent, April 1996.

[15] D. G. Goodwin. An open source, extensible software suite for CVD process simulation. In M. Allendorff, F. Maury, and F. Teyssandier, editors, *Chemical Vapor Deposition XVI and EUROCVD 14*, volume 2003-08 of *ECS Proceedings*, pages 155–162, Pennington, New Jersey, USA, 2003. The Electrochemical Society, The Electrochemical Society. URL www.cantera.org.

[16] S. Gordon and B. J. McBride. Computer program for calculation of complex chemical equilibrium composition, rocket performance, incident and reflected shocks and chapman-jouguet detonations. Technical Report NASA-SP-273, NASA, 1976.

[17] R. Grass, S. Tsantilis, and S. Pratsinis. Design of High-Temperature, Gas-Phase Synthesis of Hard or Soft TiO_2 Agglomerates. *AIChE Journal*, 52(4):1318–1325, 2006. doi:10.1002/aic.10739.

[18] J. Herzler and P. Roth. High-temperature decomposition of $ticl_4$ based on cl^- concentration measurements. *Proc. Combust. Inst.*, 29:1353–1359, 2003.

[19] D. L. Hildenbrand. Thermochemical properties of gaseous TiCl, $TiCl_2$, and $TiCl_3$. *High Temp. Mat. Sci.*, 35:151–158, 1996.

[20] D. L. Hildenbrand, K. H. Lau, and S. V. R. Mastrangelo. Gaseous species in the Ti-Al-Cl system and reaction with H_2O. *J. Phys. Chem.*, 95:3435–3437, 1991. doi:10.1021/j100161a087.

[21] O. Inderwildi and M. Kraft. Adsorption, Diffusion and Desorption of Chlorine on and from Rutile $TiO_2\{110\}$: A Theoretical Investigation. *ChemPhysChem*, 8:444–451, 2007. doi:10.1002/cphc.200600653.

[22] O. Inderwildi, D. Lebiedz, and J. Warnatz. Linear relationship between activation energies and reaction energies for coverage-dependent dissociation reactions on rhodium surfaces. *Phys. Chem. Chem. Phys*, 7:2552–2553, 2005. doi:10.1039/b506773a.

[23] O. R. Inderwildi, D. Lebiedz, O. Deutschmann, and J. Warnatz. Coverage dependence of oxygen decomposition and surface diffusion on rhodium (111): A DFT study. *J. Chem. Phys.*, 122(3):034710, 2005. doi:10.1063/1.1835891.

[24] O. R. Inderwildi, D. Lebiedz, O. Deutschmann, and J. Warnatz. Influence of Coadsorbates on the NO Dissociation on a Rhodium (311) Surface. *ChemPhysChem*, 6 (12):2513–2521, 2005. doi:10.1002/cphc.200500222.

[25] B. Karlemo, P. Koukkari, and J. Paloniemi. Formation of gaseous intermediates in titanium(IV) chloride plasma oxidation. *Plasma Chem. Plasma Process.*, 16:59–77, 1996. doi:10.1007/BF01465217.

[26] A. Kobata, K. Kusakabe, and S. Morooka. Growth and transformation of tio_2 crystallites in aerosol reactor. *AIChE J.*, 37(3):347–359, 1991. doi:10.1002/aic.690370305.

[27] M. Kraft. Modelling of Particulate Processes. *Kona, Powder and Particle*, 23:18–35, 2005.

[28] Z. Liu, X. Gong, J. Kohanoff, C. Sanchez, and P. Hu. Catalytic Role of Metal Oxides in Gold-Based Catalysts: A First Principles Study of CO Oxidation on TiO_2 Supported Au. *Phys. Rev. Lett.*, 91(26):266102, 2003. doi:10.1103/PhysRevLett.91.266102.

[29] Z.-P. Liu, S. J. Jenkins, and D. A. King. Car Exhaust Catalysis from First Principles: Selective NO Reduction under Excess O_2 Conditions on Ir. *J. Am. Chem. Soc.*, 126 (34):10746–10756, 2004. ISSN 0002-7863. doi:10.1021/ja0481833.

[30] M. Mavrikakis, J. Rempel, J. Greeley, L. Hansen, and J. Nørskov. Atomic and molecular adsorption on Rh(111). *J. Chem. Phys.*, 117(14):6737–6744, 2002. doi:10.1063/1.1507104.

[31] B. J. McBride, S. Gordon, and M. A. Reno. Coefficients for calculating thermodynamic and transport properties of individual species. Technical Report NASA-TM-4513, NASA, Glenn Research Center, Cleveland, OH, 1993. URL http://hdl.handle.net/2060/19940013151.

[32] B. J. McBride, M. J. Zehe, and S. Gordon. NASA Glenn coefficients for calculating thermodynamic properties of individual species. Technical Report TP-2002-211556, NASA, Glenn Research Center, Cleveland, OH, 2002. URL http://hdl.handle.net/2060/20020085330.

[33] N. Morgan, C. Wells, M. Goodson, M. Kraft, and W. Wagner. A new numerical approach for the simulation of the growth of inorganic nanoparticles. *J. Comput. Phys.*, 211:638–658, 2006. doi:10.1016/j.jcp.2005.04.027.

[34] H. Mühlenweg, A. Gutsch, A. Schild, and S. E. Pratsinis. Process simulation of gas-to-particle-synthesis via population balances: Investigation of three models. *Chem. Eng. Sci.*, 57:2305–2322, 2002.

[35] R. Patterson, J. Singh, M. Balthasar, M. Kraft, and J. R. Norris. The linear process deferment algorithm: A new technique for solving population balance equations. *SIAM J. Sci. Comput.*, 28(1):303–320, 2006. doi:10.1137/040618953.

[36] R. I. A. Patterson and M. Kraft. Models for the aggregate structure of soot particles. *Combust. Flame*, in press. doi:10.1016/j.combustflame.2007.04.012.

[37] S. E. Pratsinis and P. T. Spicer. Competition between gas phase and surface oxidation of $TiCl_4$ during synthesis of TiO_2 particles- a two dimensional solution of the population balance equation. *Chem. Eng. Sci.*, 53:1861–1868, 1998. doi:10.1016/S0009-2509(98)00026-8.

[38] S. E. Pratsinis, H. Bai, P. Biswas, M. Frenklach, and S. V. R. Mastrangelo. Kinetics of titanium(IV) chloride oxidation. *J. Am. Ceram. Soc.*, 73:2158–2162, 1990.

[39] M. Rasmussen, L. Molina, and B. Hammer. Adsorption, diffusion, and dissociation of molecular oxygen at defected TiO_2(110): A density functional theory study. *J. Chem. Phys.*, 120(2):988–997, 2004. doi:10.1063/1.1631922.

[40] J. Singh, R. I. A. Patterson, M. Balthasar, M. Kraft, and W. Wagner. Modelling soot particle size distribution: Dynamics of pressure regimes. Technical Report 25, c4e-Preprint Series, Cambridge, 2004.

[41] R. D. Smith, R. A. Bennett, and M. Bowker. Measurement of the surface-growth kinetics of reduced TiO_2(110) during reoxidation using time-resolved scanning tunneling microscopy. *Phys. Rev. B: Condens. Matter Mater. Phys.*, 66(3):035409, Jul 2002. doi:10.1103/PhysRevB.66.035409.

[42] P. T. Spicer, O. Chaoul, S. Tsantilis, and S. E. Pratsinis. Titania formation by $TiCl_4$ gas phase oxidation, surface growth and coagulation. *J. Aerosol Sci.*, 33:17–34, 2002. doi:10.1016/S0021-8502(01)00069-6.

[43] F. Teyssandier and M. D. Allendorf. Thermodynamics and kinetics of gas-phase reactions in the ti-cl-h system. *J. Electrochem. Soc.*, 145:2167–2178, 1998. doi:10.1149/1.1838613.

[44] S. Tsantilis and S. E. Pratsinis. Narrowing the size distribution of aerosol-made titania by surface growth and coagulation. *J. Aerosol. Sci.*, 35:405–420, 2004.

[45] M. Tutuianu, O. R. Inderwildi, W. G. Bessler, and J. Warnatz. Competitive Adsorption of NO, NO_2, CO_2, and H_2O on BaO(100): A Quantum Chemical Study. *J. Phys. Chem. B*, 110:17484–17492, 2006. doi:10.1021/jp055268x.

[46] A. Vikhansky and M. Kraft. Modelling of a RDC using a combined CFD-population balance approach. *Chem. Eng. Sci.*, 59:2597–2606, 2003. doi:10.1016/j.ces.2004.02.016.

[47] R. H. West, G. J. O. Beran, W. H. Green, and M. Kraft. First-principles thermochemistry for the production of tio_2 from $ticl_4$. *J. Phys. Chem. A*, 111(18):3560–3565, 2007. doi:10.1021/jp0661950.

[48] O. B. Willcox. Method and means for commingling and reacting fluid substances, us patent 2791490. US Patent, May 1957.

[49] P. H. Wine, J. M. Nicovich, and A. R. Ravishankara. Kinetics of the reactions of $O(^3P)$ and $O(^1D)$ with Cl_2. *J. Phys. Chem.*, 89:3914–3918, 1985. doi:10.1021/j100264a031.

[50] Y. Xiong and S. E. Pratsinis. Formation of agglomerate particles by coagulation and sintering–part i. a two-dimensional solution of the population balance equation. *J. Aerosol Sci.*, 24(3):283–300, May 1993. doi:10.1016/0021-8502(93)90003-R.